Zero-field magnetic structure in CeB_6 reinvestigated by neutron diffraction and muon spin relaxation

O. Zaharko* and P. Fischer
Laboratory for Neutron Scattering, ETHZ & PSI, CH-5232 Villigen, Switzerland

A. Schenck
Institute for Particle Physics of ETH Zürich, CH-5232 Villigen PSI, Switzerland

S. Kunii
Physics Department, Tohoku University, Sendai, Miyagi 980-8578, Japan

P.-J. Brown, F. Tasset, and T. Hansen
Institut Laue-Langevin, 156X, 38042 Grenoble Cédex, France
(Received 26 May 2003; published 1 December 2003)

The zero-field magnetic structure of $Ce^{11}B_6$ has been revised from neutron powder and single-crystal diffraction including neutron spherical polarimetry. The crystal structure remains cubic in the antiferroquadrupolar (AFQ) ordered state ($T_Q=3.3$ K, $\mathbf{k}_Q=[1/2,1/2,1/2]$) and in the antiferromagnetic (AFM) ordered state ($T_N=2.3$ K, $\mathbf{k}_1=[1/4,1/4,0]$, $\mathbf{k}_2=[1/4,-1/4,0]$, $\mathbf{k}_1'=[1/4,1/4,1/2]$, $\mathbf{k}_2'=[1/4,-1/4,1/2]$) within the precision of the experiment. The model of Effantin *et al.* [J. Magn. Magn. Mater. **47-48**, 145 (1985)] fits our 60-mK high-intensity neutron powder diffraction data rather poorly and therefore a model of the AFM multi-**k** structure has been developed. It is a 2 $\mathbf{k}-\mathbf{k}'$ transverse sine-wave structure with the Ce magnetic moments strictly along $[1-10]$ and $[110]$ and orthogonal arrangement of the nearest moments. Ce atoms located at the $z=0$ and $z=1$ layers have significantly different magnetic moment values. In addition there is a modulation of the moment value in each layer. The resulting ordered magnetic Ce moments reach $0.744(16)\mu_B$, $0.543(16)\mu_B$ at $z=1$ and only $0.01\mu_B$, $0.138(7)\mu_B$ at $z=0$ at 60 mK. This complex AFM structure is due to competition between the established AFQ order and the dipolar and octupolar AFM order developing at lower temperatures. The model is consistent with the μSR zero-field results [R. Feyerherm *et al.*, J. Magn. Magn. Mater. **140-144**, 1175 (1995)] and suggests a highly inhomogeneous conduction electron spin polarization and anisotropic RKKY interactions below T_N.

DOI: 10.1103/PhysRevB.68.214401 PACS number(s): 75.25.+z, 71.27.+a

I. INTRODUCTION

Due to multipolar interactions, the dense Kondo CeB_6 compound with a cubic CaB_6-type structure (space group $Pm\bar{3}m$) has an unusual magnetic-field—temperature phase diagram.[1,2] At $T_Q=3.3$ K in zero external magnetic field CeB_6 undergoes a transition from the paramagnetic (phase I) to the antiferroquadrupole (AFQ) state (phase II). At $T_N=2.3$ K antiferromagnetic (AFM) ordering (phase III) takes place. The AFQ phase is associated with the wave vector $\mathbf{k}_Q=[1/2,1/2,1/2]$ according to neutron diffraction in applied magnetic field[2] and x-ray resonant scattering experiments in zero field.[3,4] T_Q increases with applied magnetic field which is unusual[5] and the temperature dependence of the induced AFM moment is peculiar.[6] In order to explain the neutron, NMR and muon spin relaxation (μSR) results consistently in the AFQ phase, the interactions between the dipole, quadrupole, and octupole Ce moments have to be taken into account. The Γ_5-type (O_{yz}, O_{zx}, O_{xy}) quadrupolar ordering takes place in zero field, the O_{xy} order is stabilized by a magnetic field applied along $[001]$, and $O_{yz}+O_{zx}$ order is predicted for $H\|[110]$ and $O_{xy}+O_{yz}+O_{zx}$ order for $H\|[111]$.[7,8] It appears that the T_{xyz}-type octupolar interaction[6,9–11] is particularly strong and almost independent of the field direction. Its consideration solves the discrepancy between the types of AFQ order proposed from NMR and neutron experiments.[9,10] The peculiar behavior of the magnetic intensity in magnetic field below T_Q can be explained by competition between the dipolar exchange coupling and the AFM coupling of the T_{xyz}-type octupolar moments.[6]

Theoretical models[8,12,13] suggest that the AFQ ordering should introduce distortions of the crystal lattice. These distortions are expected to be quite small due to weak coupling of the quadrupole moment to the lattice strain, which has different symmetry.[14] No clear experimental evidence for these distortions has been obtained up to now.[3]

Another point is that polarized neutron, NMR, and μSR studies[15–18] indicate that the anisotropic electron density distribution and complex interactions between Ce multipoles induce substantial (up to 30%) magnetization density at the boron framework. The existence of the anisotropic hybridization of the $2p$ states of boron and the $4f$ electrons of Ce explained the hyperfine field at the boron sites in the NMR experiment.[16,17] The field-induced magnetization near or inside the B_6 molecule can also explain the μSR results[18] in the AFQ phase of CeB_6. It is however claimed[19] that the interpretation of polarized neutron diffraction by Saitoh *et al.*[15] is biased by systematic errors and that the magnetization is localized on the Ce sites only.

 ©2003 The American Physical Society

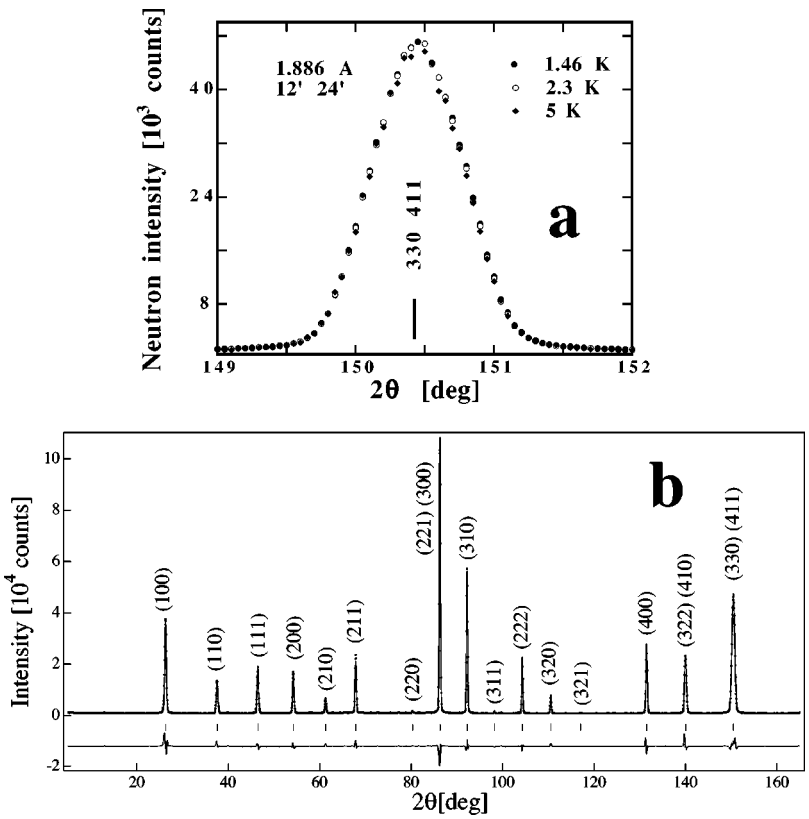

FIG. 1. High-resolution HRPT neutron powder diffraction data of $Ce^{11}B_6$ measured with $\lambda = 1.886$ Å: (a) (330) and (411) reflections at 5 K (paramagnetic regime), 2.3 K (AFQ state), 1.46 K (AFM state), (b) fit to the cubic CaB_6-type crystal structure at 2.6 K.

The low-temperature AFM regime below T_N is also still not sufficiently understood. The AFM phase of CeB_6 orders with the wave vectors $\mathbf{k}_1=[1/4,1/4,0]$, $\mathbf{k}_2=[1/4,-1/4,0]$, $\mathbf{k}_1'=[1/4,1/4,1/2]$, and $\mathbf{k}_2'=[1/4,-1/4,1/2]$. According to the neutron diffraction in applied magnetic fields[20] these four vectors vanish and appear at the same temperature and at the same field; i.e., they describe the magnetic structure within one domain resulting in so-called double $\mathbf{k}-\mathbf{k}'$ structure. Such $2\mathbf{k}-\mathbf{k}'$ structure with two distinct wave vectors is unusual and cannot be stabilized by exchange interactions only.[23] Effantin *et al.*[2] suggested a transverse sine-modulated noncollinear magnetic structure with magnetic moments aligned along the $[1-10]$ and $[110]$ directions for $\mathbf{k}_1$ and $\mathbf{k}_1'$. The amplitudes of the waves associated with $\mathbf{k}_1$ and $\mathbf{k}_1'$ vectors were reported to be almost equal and the resulting ordered magnetic moment was $0.28(6)\mu_B$ at 1.3 K. This model, however, fails to explain the zero-field μSR results[24,25]: it would yield only three different values of internal fields, while experimentally eight spontaneous precession frequencies were found. The largest frequency of 76 MHz deduced from μSR data would require an ordered moment value of at least $0.75\mu_B$. In addition two of the frequencies exhibit peculiar temperature dependences for $T \leqslant 1$ K. Other models, such as a helical structure with magnetic moments in the (001) plane and sine-modulated structures with moments along $\langle 111\rangle$ or $\langle 100\rangle$,[1,26] also fail to explain the μSR results.

To resolve the discrepancy between neutron and μSR experiments in the AFM phase of CeB_6, we have carried out a detailed neutron diffraction study of CeB_6 at low temperatures. We obtained information on the crystal structure in the 1.5–8 K temperature interval, determined the direction of the Ce magnetic moments, derived a novel model of the AFM structure of CeB_6 consistent with the μSR results, and measured the temperature dependence of the AFM intensities in the temperature range from 36 mK to 2.3 K.

II. EXPERIMENTAL DETAILS

High-quality powder and a single crystal of $Ce^{11}B_6$ enriched with ^{11}B isotope were prepared in Tohoku University by the floating zone method. The ^{11}B isotope content was 99.7 at.% ^{11}B for the powder and 99.52 at.% ^{11}B for the single crystal, which led to a rather moderate absorption coefficient, 0.754 cm^{-1} for the powder and 1.994 cm^{-1} for the single crystal at 1.886 Å neutron wavelength. The size of the samples was optimized to facilitate the absorption correction. The powder was packed into cylindrical V or Al containers with $\emptyset = 6$-8 mm; the single crystal had cylindrical shape and dimensions $\emptyset = 6.3$ mm, $h = 7$ mm. Neutron powder diffraction in the high-resolution mode was performed at the HRPT diffractometer at SINQ, Switzerland. Wavelengths of 1.886 Å, 1.197 Å and collimations $\alpha_1 = 12'$, $\alpha_2 = 24'$ were used. The sample was cooled in an ILL orange cryostat to 1.5 K. High-intensity neutron powder patterns were collected at the D20 instrument at ILL, France, with a wavelength of 2.421 Å. This experiment was performed using a ^{3}He/^{4}He dilution refrigerator in the temperature interval from 60 mK to 5 K. Both diffractometers are equipped with 1600 detectors, covering a range of 160° scattering angle. Rietveld refinement of the crystal and magnetic structures was performed using the FULLPROF program.[27] Single-crystal

unpolarized neutron diffraction was performed on the TriCS diffractometer at SINQ with $\lambda = 1.18$ Å. The temperature dependence of two magnetic peaks in the regime from 36 mK to 2.3 K was measured in a ^{3}He/^{4}He dilution refrigerator with a ^{3}He area detector. Spherical neutron polarimetry (SNP) on the $Ce^{11}B_6$ single crystal was carried out at the IN20 spectrometer at ILL with $\lambda = 2.36$ Å. The crystal was mounted with the $[1-10]$ direction vertical inside an ILL orange cryostat placed in the annular zero-field space of Cryopad II (Ref. 28) and cooled down to 1.6 K.

III. RESULTS AND DISCUSSION

A. Crystal structure of CeB_6 at low temperatures ($\leqslant$8 K)

Information about the crystal symmetry and atomic displacements is very valuable for understanding the ordering of the quadrupolar moments. We tried to find these weak distortions in $Ce^{11}B_6$ by means of high-resolution neutron powder diffraction. The (330), (411) reflections measured with the highest resolution of the HRPT instrument[29] with $\lambda = 1.886$ Å are presented in Fig. 1(a). No evidence of splitting or even broadening of the Bragg peak in the AFQ and AFM regimes can be seen. Figure 1(b) presents results of a Rietveld refinement of the crystal structure within the cubic CaB_6-type structure at 2.6 K. The agreement is quite good, yielding the weighted profile agreement R factor $R_{wp} = 9.5\%$ and $R_{Bragg} = 5.2\%$ concerning integrated intensities. Allowing the symmetry to relax led to the angle $\alpha = 90.005(3)°$ in the case of the rhombohedral distortion and to the lattice constants $a = b = 4.1368(2)$ Å, $c = 4.1366(3)$ Å in the case of the tetragonal distortion. Thus, the crystal lattice is cubic within the precision of the experiment.

The temperature variation of the cubic lattice constant a of CeB_6 in the 1.5–8 K temperature range is presented in Fig. 2(a). It had been determined from high-intensity data measured with $\lambda = 1.197$ Å—i.e., with increased momentum transfer range ($\sin\theta/\lambda \leqslant 0.82$ Å^{-1}). The lattice expands with decreasing temperature in the paramagnetic state at $T > T_Q$, contracts in the AFQ phase, in full accord with theoretical studies,[11] and changes very subtle below T_N. The change of a is very small; the $\Delta a/a$ ratio is less than 1.5×10^{-5}. This value is in the order of the thermal expansion coefficient measured by Schefzyk *et al.*[30]

Finally we tried to obtain the atomic parameters from data collected at $\lambda = 1.197$ Å. The O_{xy}-type AFQ order must break the inversion symmetry of B_6 octahedra and a displacement of B atoms must be present.[8] We failed to detect any variation of the x coordinate of the B atoms with temperature within the experimental precision $[x_B = 0.1983(2)]$. The isotropic thermal parameters of Ce and B atoms, presented in Fig. 2(b), exhibit a temperature variation similar to the variation of the lattice constant. To detect such weak distortions and related atomic displacements in CeB_6 at zero field, experiments with shorter wavelength and/or high-resolution synchrotron x-ray investigations are required.

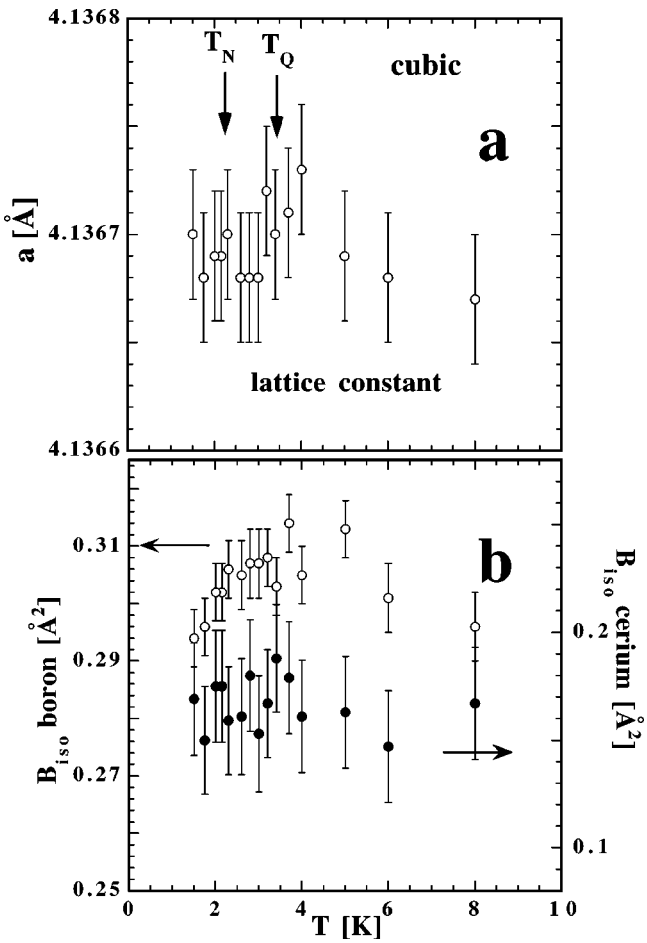

FIG. 2. Thermal variation of the lattice constant of $Ce^{11}B_6$ (top) and isotropic thermal parameters of the cerium and boron atoms refined from $\lambda = 1.12$ Å HRPT data in the 1.5–8 K regime.

B. Magnetic structure of CeB_6 below T_N

To revise the AFM structure we first collected high-intensity neutron powder diffraction patterns with neutron wavelength $\lambda = 2.421$ Å at the D20 diffractometer at the temperatures 3.8 K, 2.6 K, 1.7 K, and 0.06 K. As the AF magnetic intensities were very weak compared to the nuclear ones [the strongest magnetic peak had only 3000 counts in the peak maximum compared to 1.75×10^6 counts of the nuclear peak (1 0 0)], measuring time of the order of 6 h was needed to get acceptable statistics. We analyzed magnetic difference patterns to the one obtained in the paramagnetic state at 3.9 K. They are shown in Fig. 3. The difference pattern for 2.6 K in the AFQ state also shows neither magnetic nor nuclear superstructure peaks such as (1/2 1/2 1/2) in accordance with HRPT results. The AFM reflections at $T < T_N$ could be indexed with the wave vectors $\mathbf{k}_1 = [1/4,1/4,0]$ and $\mathbf{k}_1' = [1/4,1/4,1/2]$.[31]

For the magnetic structure refinement the magnetic neutron intensities were normalized via the scale factor obtained from a profile fit of the nuclear neutron diffraction pattern measured at 3.8 K. The 60 mK and 1.7 K difference patterns contained additional intensity at nuclear positions[32] and peaks at high scattering angles 2θ corresponding to intense scattering from aluminum parts of the ILL cryostat. Due to

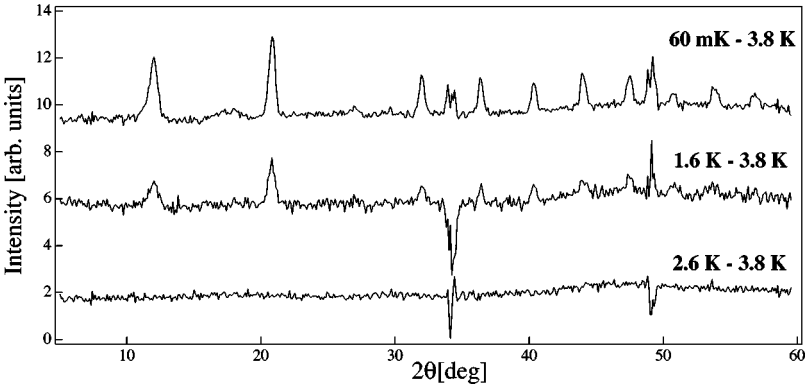

FIG. 3. Observed magnetic difference D20 patterns of $Ce^{11}B_6$: bottom, $I(2.6\ \mathrm{K})$-$I(3.8\ \mathrm{K})$; middle, $I(1.6\ \mathrm{K})$-$I(3.8\ \mathrm{K})$; top, $I(60\ \mathrm{mK})$-$I(3.8\ \mathrm{K})$.

that and in view of the decrease of the magnetic Ce^{3+} form factor with 2θ, only the range of $[8°–64°]$ of the difference patterns was used. The Effantin model gave a rather poor fit to our experimental data. Modification of this model—i.e., the introduction of two sublattices with different magnetic moment values associated with the $\mathbf{k}_1$ and $\mathbf{k}_1'$ wave vectors—did not give significant improvement. Other models with magnetic moments along $\langle 111\rangle$ and $\langle 100\rangle$ yield even worse agreement.

Therefore, we decided to limit the range of possible new models by performing a neutron spherical polarimetry experiment on the above-mentioned $Ce^{11}B_6$ single crystal. It is a powerful method,[28,33] allowing us to distinguish magnetic from nuclear scattering, to determine the direction of magnetic moments, and to distinguish between different magnetic arrangements. A number of reflections at 1.6 K were examined with CRYOPAD II at the IN20 spectrometer with $\lambda = 2.36$ Å. The polarization of the scattered neutrons was analyzed for three directions of polarization of the incoming beam. The local coordinate system was chosen such that the x axis is along the scattering vector of a reflection, z is in the vertical direction, and the magnetic interaction vector $\mathbf{M}\perp(\mathrm{Q})$ lies in the yz plane. Analysis of AF magnetic reflections (Table I) showed that the directions of the incident and scattered polarization are antiparallel for x and y and parallel for z within experimental error. This shows that there is no component of the magnetic interaction vector along y in the horizontal plane for any of the observed reflections; it is always vertical along z (the $[1-10]$ direction of the crystal). In addition no significant depolarization of the scattered beam occurs. These observations prove that the scattering is purely magnetic and that $\mathbf{M}\perp(\mathrm{Q})$ for $\pm h \pm hl$ reflections points strictly in the $[1-10]$ direction; i.e., the direction of magnetic moments is perpendicular to the corresponding wave vector. Analysis of several nuclear reflections confirmed that there is no ferromagnetic component. Some weak intensity at the AFQ (1/2 1/2 1/2) position was also detected. Interestingly, it was found to be fully depolarized. Such intensity could be due to coupling of either the magnetization distribution or the structural environment to the quadrupolar order, but in neither case should it be fully depolarized for all three directions of incident polarization. We therefore concluded that the intensity observed at the (1/2 1/2 1/2) position was due to unpolarized half-wavelength neutrons not completely removed by the graphite filter in the scattered beam.

Next we tried to develop a model of the AF magnetic structure based on symmetry analysis[34] and available experimental observations. We started with the space group $Pm\overline{3}m(O_h^1)$ of the paramagnetic state, as symmetry lowering

TABLE I. Results of the polarization analysis of AFM reflections from $Ce^{11}B_6$ single crystal. P_{xx}, P_{xy}, and P_{xz} are the polarizations of the scattered beam in the x, y, and z directions for the incident beam polarized along x, etc.

h	k	l	P_{xx}	P_{xy}	P_{xz}	P_{yx}	P_{yy}	P_{yz}	P_{zx}	P_{zy}	P_{zz}
−0.25	−0.25	0.0	−0.906(10)	−0.070(14)	−0.123(13)	0.069(13)	−0.945(10)	0.045(13)	−0.043(13)	0.032(14)	0.925(7)
−0.25	−0.25	0.5	−0.922(5)	0.001(11)	−0.025(11)	0.012(10)	−0.907(6)	0.091(11)	−0.006(10)	0.046(11)	0.936(5)
0.25	0.25	0.0	−0.920(9)	−0.017(13)	0.112(13)	0.025(13)	−0.891(10)	0.004(14)	0.073(13)	−0.060(13)	0.909(8)
0.25	0.25	0.5	−0.917(8)	−0.049(14)	0.053(14)	0.038(14)	−0.936(7)	0.070(13)	0.090(14)	0.073(14)	0.894(7)
−0.25	−0.25	1.0	−0.891(13)	−0.045(20)	0.035(20)	0.058(20)	−0.926(13)	0.068(20)	0.018(20)	0.117(21)	0.943(13)
−0.25	−0.25	1.5	−0.913(19)	−0.003(25)	0.021(26)	−0.021(24)	−0.963(17)	0.110(24)	0.006(25)	0.042(25)	0.910(16)
−0.75	−0.75	0.0	−0.891(36)	0.037(43)	−0.086(41)	0.058(38)	−0.838(32)	0.053(37)	−0.072(41)	−0.063(38)	0.856(33)
−0.75	−0.75	0.5	−0.925(14)	−0.017(21)	−0.092(21)	0.063(21)	−0.925(13)	0.098(21)	−0.060(21)	0.106(21)	0.970(15)
0.75	0.75	0.0	−0.827(37)	−0.062(45)	0.088(45)	0.000(48)	−0.932(45)	−0.133(47)	0.101(46)	−0.068(44)	0.866(39)
0.75	0.75	0.5	−0.847(63)	−0.002(64)	0.084(69)	0.168(58)	−0.879(58)	−0.098(63)	0.091(60)	−0.058(60)	0.957(54)
−0.75	−0.75	1.0	−0.929(22)	0.020(26)	−0.141(27)	−0.013(26)	−0.876(21)	0.066(26)	−0.022(26)	0.129(26)	0.924(20)
−0.75	−0.75	1.5	−0.937(21)	0.007(26)	−0.072(26)	0.010(26)	−0.893(21)	0.022(26)	−0.073(25)	0.091(26)	0.889(18)
−0.75	−0.75	2.0	−0.951(27)	−0.008(35)	−0.048(35)	−0.016(35)	−0.893(26)	0.101(35)	0.090(35)	0.077(35)	0.910(28)

TABLE II. Irreducible representations of the space group $Pm\overline{3}m$ for $\mathbf{k}_1=[1/4,1/4,0]$, $\mathbf{k}_2=[1/4,-1/4,0]$, $\mathbf{k}'_1=[1/4,1/4,1/2]$, and $\mathbf{k}'_2=[1/4,-1/4,1/2]$ and corresponding magnetic mode basis functions $\boldsymbol{\psi}$, as obtained from program MODY (Ref. 22).

$\mathbf{k}_1$, $\mathbf{k}'_1$	$\mathbf{e}$	2_{110}	m_z	m_{1-10}	$\boldsymbol{\psi}$ for $\mathbf{k}_1$, $\mathbf{k}'_1$	$\boldsymbol{\psi}$ for $-\mathbf{k}_1$, $-\mathbf{k}'_1$
τ_1	1	1	1	1		—
τ_2	1	1	−1	−1	$\mathbf{e}_x+\mathbf{e}_y$	$-(\mathbf{e}_x+\mathbf{e}_y)$
τ_3	1	−1	1	−1	$\mathbf{e}_z$	$\mathbf{e}_z$
τ_4	1	−1	−1	1	$\mathbf{e}_x-\mathbf{e}_y$	$-(\mathbf{e}_x-\mathbf{e}_y)$
$\mathbf{k}_2$, $\mathbf{k}'_2$	$\mathbf{e}$	2_{1-10}	m_z	m_{110}	$\boldsymbol{\psi}$ for $\mathbf{k}_2$, $\mathbf{k}'_2$	$\boldsymbol{\psi}$ for $-\mathbf{k}_2$, $-\mathbf{k}'_2$
τ_1	1	1	1	1		—
τ_2	1	1	−1	−1	$\mathbf{e}_x-\mathbf{e}_y$	$-(\mathbf{e}_x-\mathbf{e}_y)$
τ_3	1	−1	1	−1	$-\mathbf{e}_z$	$-\mathbf{e}_z$
τ_4	1	−1	−1	1	$\mathbf{e}_x+\mathbf{e}_y$	$-(\mathbf{e}_x+\mathbf{e}_y)$

in the AFQ phase was not detected. Each of the stars of $\mathbf{k}$ and $\mathbf{k}'$ contain 12 arms—for example, for the star $\mathbf{k}$, $\pm\mathbf{k}_1=\pm[1/4,1/4,0]$, $\pm\mathbf{k}_2=\pm[1/4,-1/4,0]$, $\pm\mathbf{k}_3=\pm[1/4,0,1/4]$, $\pm\mathbf{k}_4=\pm[1/4,0,-1/4]$, $\pm\mathbf{k}_5=\pm[0,1/4,1/4]$, and $\pm\mathbf{k}_6=\pm[0,1/4,-1/4]$. From powder neutron diffraction it is not possible to distinguish between magnetic single- and multiple-$\mathbf{k}$ structures. But previous single-crystal neutron diffraction[20] in applied magnetic field showed that the magnetic structure is of the $2\mathbf{k}-\mathbf{k}'$ type (see the Introduction). Therefore, we restricted our analysis to the $\mathbf{k}_1$, $\mathbf{k}_2$ and $\mathbf{k}'_1$, $\mathbf{k}'_2$ wave vectors only.

The four real, one-dimensional irreducible magnetic representations τ_1, τ_2, τ_3, and τ_4 of the $Pm\overline{3}m$ space group for the $\mathbf{k}_1$, $\mathbf{k}_2$ and $\mathbf{k}'_1$, $\mathbf{k}'_2$ wave vectors and the corresponding basis vectors are listed in Table II. For the τ_2 irreducible representation the basis vectors for $\mathbf{k}_1$ are along [110]—i.e., the direction of magnetic moments is along the wave vector—which contradicts the NSP experiment. For τ_4 the basis vectors are along [1−10]; i.e., the direction of magnetic moments is transversal to the wave vector. Therefore, we restricted analysis to τ_4. The possible models of the magnetic structure may be obtained as linear combinations of basis vectors:

$$\mathbf{S}_n=\sum_{\nu\eta} C^{\nu\eta}\boldsymbol{\psi}^{\nu\eta}, \tag{1}$$

where ν and η number the representation and arms of the $\mathbf{k}$ vector, $C^{\nu\eta}$ are the mixing coefficients, and $\boldsymbol{\psi}^{\nu\eta}$ are the basis vectors. Moreover, considering the magnetic moments as complex axial vectors, the Fourier components of those in the nth chemical cell are related to ones in the "zero" cell by the equation[21]

$$\mathbf{S}_{nj}=\mathbf{S}_{0j}e^{i\Phi(n)}, \tag{2}$$

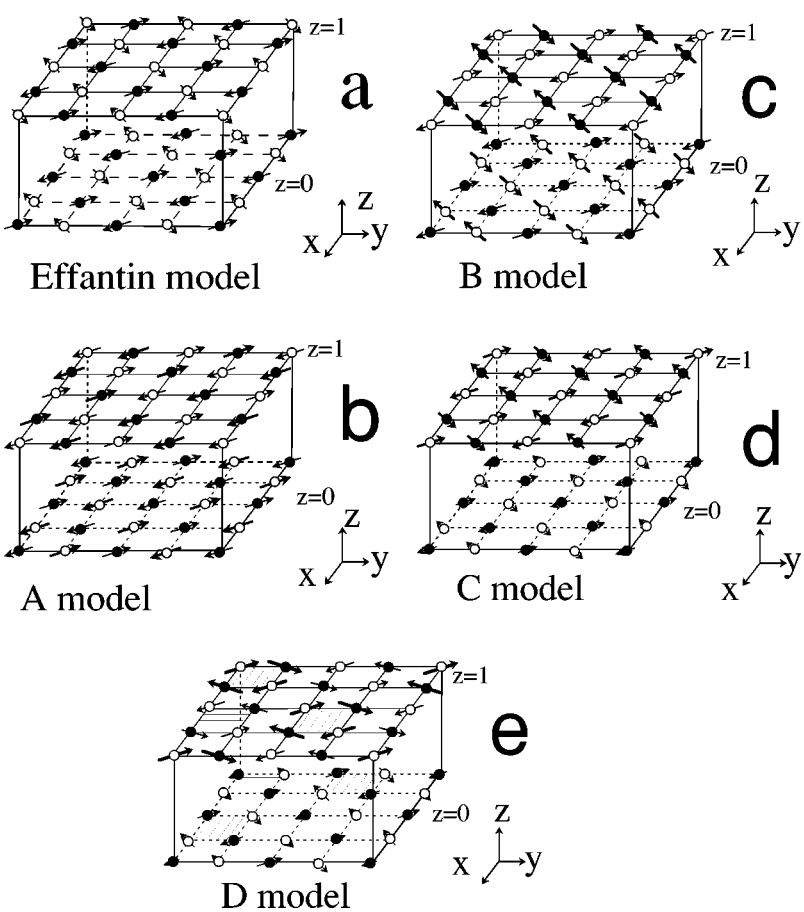

FIG. 4. Possible AFM structures of CeB_6 with only Ce atoms presented. The AFQ ordering scheme is shown by black and white circles. (a) Effantin model, (b) model *A*, (c) model *B*, (d) model *C*, and (e) model *D*.

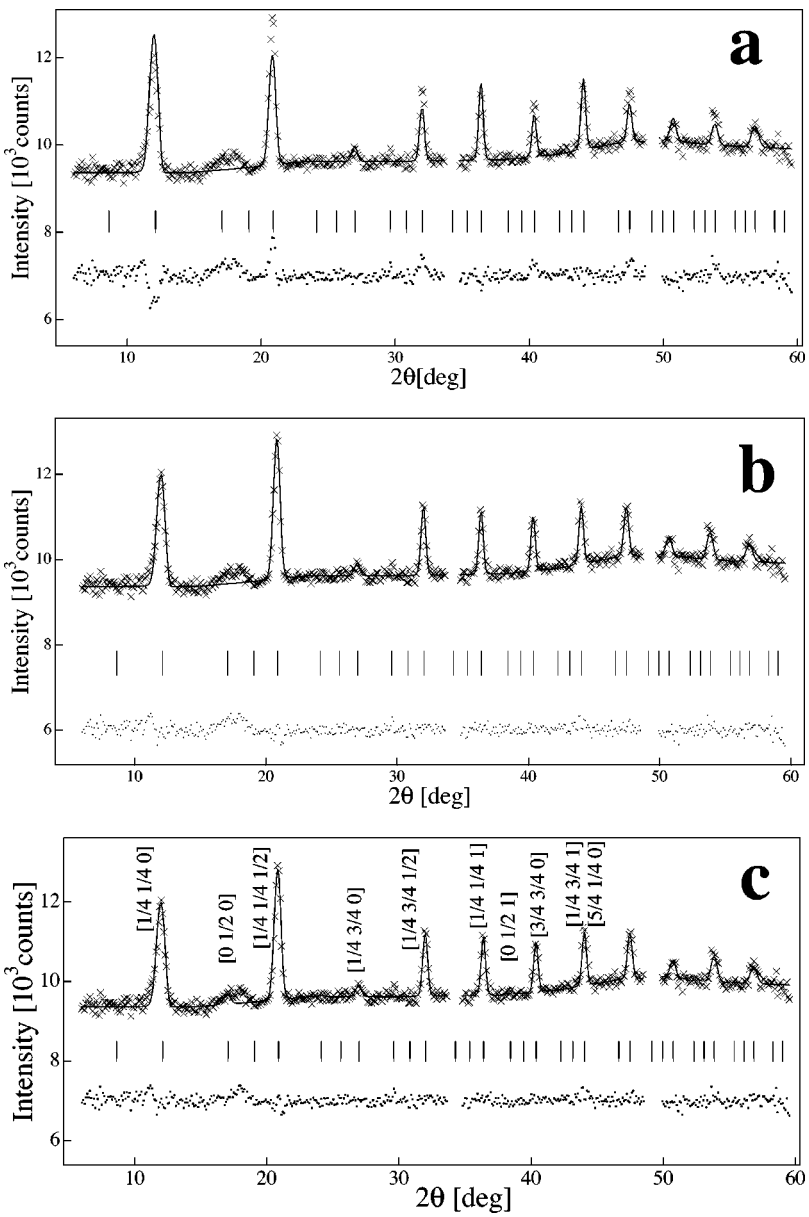

FIG. 5. Observed (renormalized) magnetic difference D20 pattern $I(60\ \mathrm{mK})$-$I(3.8\ \mathrm{K})$, calculated and difference patterns of $Ce^{11}B_6$ denoted by crosses, solid, and dotted lines, respectively. (a) Effantin model, (b) model *C*, and (c) model *D*. The indices of reflections presented in (c) are valid also for (a) and (b).

where $\Phi(n)=2\pi\mathbf{k}\mathbf{t}(n)$, and $\mathbf{t}(n)$ is a translation vector from the 0 cell to the *n* cell. In general such relations with $e^{i2\pi\mathbf{k}\mathbf{t}(n)}$ factors are not real quantities and thus cannot represent magnetic moments. To obtain real values, one has to use both $\mathbf{k}$ and $-\mathbf{k}$.

In our case the τ_4-modulated magnetic moment arrangements can be described as

$$\begin{aligned}\mathbf{S}_n=&\,\mu_1\mathbf{e}_{[1,-1,0]}\cos[2\pi\mathbf{k}_1\mathbf{t}(n)+\phi_1]\\&+\mu_2\mathbf{e}_{[1,-1,0]}\cos[2\pi\mathbf{k}_1'\mathbf{t}(n)+\phi_2]\\&+\mu_3\mathbf{e}_{[1,1,0]}\cos[2\pi\mathbf{k}_2\mathbf{t}(n)+\phi_3]\\&+\mu_4\mathbf{e}_{[1,1,0]}\cos[2\pi\mathbf{k}_2'\mathbf{t}(n)+\phi_4],\end{aligned}\tag{3}$$

where $\mathbf{e}_{[1,-1,0]}$ and $\mathbf{e}_{[1,1,0]}$ are unit vectors along the directions $[1-10]$ and $[110]$. $\mathbf{t}(n)$ are the cell translations, and μ_{1-4} and ϕ_{1-4} are the magnetic moment amplitudes and phases.

We tried to construct magnetic structures within the τ_4 representation based on the NaCl type antiferroquadrupolar configuration of CeB_6 II. However, the fit to measured magnetic powder neutron intensities was poor. It is worth mentioning that the Effantin model [Fig. 4(a)],[2] discussed above, also belongs to the τ_4 representation. It is obtained within the assumption that $\mu_1=\mu_2=\mu_3=\mu_4$ and $\phi_1=-\pi/4$, $\phi_2=\phi_3=\pi/4$, and $\phi_4=3\pi/4$:

$$\begin{aligned}\mathbf{S}_n=&\,\mu_1\mathbf{e}_{[1,-1,0]}\cos[2\pi\mathbf{k}_1\mathbf{t}(n)-\pi/4]\\&+\mu_1\mathbf{e}_{[1,-1,0]}\cos[2\pi\mathbf{k}_1'\mathbf{t}(n)+\pi/4]\\&+\mu_1\mathbf{e}_{[1,1,0]}\cos[2\pi\mathbf{k}_2\mathbf{t}(n)+\pi/4]\\&+\mu_1\mathbf{e}_{[1,1,0]}\cos[2\pi\mathbf{k}_2'\mathbf{t}(n)+3\pi/4].\end{aligned}\tag{4}$$

However, the Effantin model is not consistent with our neutron powder diffraction data [Fig. 5(a)] and results in only

TABLE III. Models of the AFM structure of CeB_6 and their conformity to experimental data. μ is the ordered magnetic moment of Ce atoms, R_m the magnetic reliability factor, χ^2 the goodness of fit to magnetic difference D20 neutron diffraction patterns, and F number of muon frequencies produced by the corresponding model.

	Effantin	A	B	C	D
60 mK	0.442(3)	0.403(3)	0.403(3)	0.643(4)	0.744(16)
μ [μ_B/Ce]	-	0.506(4)	0.506(4)	0.073(4)	0.543(16)
					0.01[a]
					0.138(7)
R_m [%]	19.5	11.2	11.2	11.2	15.5
χ^2	3.4	1.9	1.9	1.9	1.8
1.7 K	0.310(5)	0.269(7)	0.269(7)	0.454(7)	0.462(37)
μ [μ_B/Ce]	-	0.374(7)	0.374(7)	0.074(7)	0.449(37)
					0.01[a]
					0.141(13)
R_m [%]	35	26	26	26	27
χ^2	1.4	1.1	1.1	1.1	1.1
k multiplicity	$2\mathbf{k}-\mathbf{k}'$	$\mathbf{k}-\mathbf{k}'$	$\mathbf{k}-\mathbf{k}'$	$2\mathbf{k}-\mathbf{k}'$	$2\mathbf{k}-\mathbf{k}'$
F	3	4	4	5	8

[a]This small, for the neutron intensities almost negligible value has been fixed as required by μSR, yielding good convergence of the neutron refinement.

three spontaneous precession μSR frequencies instead of eight measured.[25]

Under assumption that the magnetic structure can deviate from the arrangement imposed by the NaCl-type antiferroquadrupolar configuration of CeB_6 II we found a number of models within the τ_4 representation fitting the D20 60 mK−3.8 K difference neutron powder data equally well. This is related to the fact that the phases corresponding to different $\mathbf{k}$ vectors cannot be determined from the measured neutron intensities. Only for special choices of the phases such as in the subsequently discussed models A and B does one obtain constant moment magnitudes in the commensurate magnetic unit cell. More general choices of the phases imply variation of the moment magnitudes in the magnetic unit cell. Therefore additional information such as from μSR is needed to distinguish between the models.

The most appropriate models are presented in Table III and Fig. 4. We introduce them with increase of complexity—from a simplest to a most complex one. The simplest one, a modulated magnetic structure A with $\mu_1 \neq \mu_2 \neq 0$, $\mu_3 = \mu_4 = 0$ and $\phi_1 = 0, \phi_2 = \pi/2$,

$$\mathbf{S}_n = \mathbf{e}_{[1,-1,0]}\mu_1 \cos[2\pi \mathbf{k}_1 \mathbf{t}(n)] + \mu_2 \cos[2\pi \mathbf{k}_1' \mathbf{t}(n) + \pi/2], \tag{5}$$

is illustrated in Fig. 4(b). This model involves only $\pm\mathbf{k}_1$ and $\pm\mathbf{k}'_1$ wave vectors and yields two collinear Ce sublattices with different magnetic Ce moments $\mu_1 = 0.403(3)\mu_B$ and $\mu_2 = 0.506(4)\mu_B$. It implies ferro- (F) and antiferro- (AF) magnetic couplings along the z axis for moments at $(00z)$ and $(10z)$, respectively.

Another simple model B is obtained for $\mu_1 \neq \mu_4 \neq 0$, $\mu_2 = \mu_3 = 0$ and $\phi_1 = 0, \phi_4 = -\pi/2$:

$$\mathbf{S}_n = \mu_1 \mathbf{e}_{[1,-1,0]} \cos[2\pi \mathbf{k}_1 \mathbf{t}(n)] + \mu_4 \mathbf{e}_{[1,1,0]} \cos[2\pi \mathbf{k}'_2 \mathbf{t}(n) - \pi/2]. \tag{6}$$

It is illustrated in Fig. 4(c). This model involves $\mathbf{k}_1$ and $\mathbf{k}'_2$ wave vectors and yields two perpendicular sublattices. The magnetic Ce moments values and the couplings along the z axis are the same as for model A. In the basal plane such a model with $\mu_1 = \mu_4$ is equivalent to the four-sublattice model of Sera and Kobayashi.[11] The latter also explains easy directions of magnetization $\langle 110 \rangle$. Models A and B are in agreement with high-intensity neutron powder diffraction ($R_m = 11.2\%$) and neutron spherical polarimetry. However, they contradict single-crystal neutron diffraction at applied field (Ref. 20) and zero-field μSR (Ref. 25): the models are of the $\mathbf{k}-\mathbf{k}'$ type and they result in only four spontaneous precession μSR frequencies instead of eight measured.

Better agreement with μSR can be achieved under assumption that more than two magnetic Ce moment amplitudes exist in the magnetic unit cell—i.e., by splitting the Ce site into two sites, one at $z=0$ and another at $z=1$. The magnetic arrangement is described as

$$\mathbf{S}_n = \mu_1 \mathbf{e}_{[1,-1,0]} \cos[2\pi \mathbf{k}_1 \mathbf{t}(n)] + \mu_2 \mathbf{e}_{[1,-1,0]} \cos[2\pi \mathbf{k}'_1 \mathbf{t}(n)] + \mu_3 \mathbf{e}_{[1,1,0]} \cos[2\pi \mathbf{k}_2 \mathbf{t}(n) + \pi/2] + \mu_4 \mathbf{e}_{[1,1,0]} \cos[2\pi \mathbf{k}'_2 \mathbf{t}(n) - \pi/2]. \tag{7}$$

The corresponding model C with perpendicular sublattices is presented in Fig. 4(d). It has two different magnetic moment values: a very small one $0.073(4)\mu_B$ in the $z=0$ layer and a larger one $0.643(4)\mu_B$ at $z=1$. As we argue later, this layered magnetic structure is related to competition between the AFM dipolar, octupolar, and AF quadrupolar ordering. The model is of the $2\mathbf{k}-\mathbf{k}'$ type and it results in the same fit of the D20 neutron data as the A and B models [$R_m = 11.2\%$, Fig. 5(b)]. The agreement of model C with the μSR results is, however, not satisfactory, as such a magnetic moment arrangement would yield only five precession frequencies.

To have eight different values of internal fields the magnetic structure should be even more complicated. For this either a more complex arrangement of magnetic moments or different moment values should be present. We did not succeed in finding another arrangement of moments consistent with all experimental observations, but a further split of moment values by introducing amplitude modulation in the layers was successful. In model D the magnetic moment arrangement is the same as in model C [Eq. (7)] and the moment modulation within each layer is described as

$$P = P_0 + P_1\{\mathbf{e}_{[1,1,0]} \cos[2\pi \mathbf{k}_1 \mathbf{t}(n)] + \mathbf{e}_{[1,-1,0]} \cos[2\pi \mathbf{k}_2 \mathbf{t}(n) - \pi/2]\}. \tag{8}$$

The average moment value P_0 within the layer is equal to $0.073\mu_B$ for $z=0$ and $0.640\mu_B$ for $z=1$; these values coincide with the magnetic moments from model C. The maximal deviation P_1 of the moment within the layer—i.e., the

amplitude of modulation—is $-0.065\mu_B$ for $z=0$ and $0.064\mu_B$ for $z=1$. This model results in eight sublattices and four different magnetic moment values, which at 60 mK are $0.01\mu_B$, $0.136(7)\mu_B$ for $z=0$ and $0.744(16)\mu_B$, $0.543(16)\mu_B$ for $z=1$. The model is presented in Fig. 4(e). To distinguish the different moments within the same layer we used dashed squares to connect the moments of equal value. Dashes along x correspond to higher moment values and dashes along y to lower moment values.

The agreement between this model and the D20 60 mK−3.8 K difference neutron powder data is presented in Fig. 5(c). The R value of magnetic reflections is $R_m=15.5\%$ and the goodness of fit $\chi^2=1.8$. Actually it is not possible to give preference to model C or D based on the quality of the refinement only. The R value of magnetic reflections is slightly worse for model D. But the goodness of fit χ^2 is better for model D. This is because model D gives rise to weak hkl reflections with $k=1/2$. These reflections should be described by a new wave vector [0 1/2 0], which implies additional, very weak modulation. The calculated intensity of the (0 1/2 0) reflection is very small, only 8% of the (1/4 1/4 0) reflection. Interestingly, the (0 1/2 0) reflection corresponds to a broad maximum [see Fig. 5(c)] in the powder diffraction pattern not explained by other models. The broadening indicates short range of the magnetic correlations associated with this additional modulation. To check the correctness of the proposed model a high-intensity single-crystal experiment is desirable. Presently we give preference to model D as it gives satisfactory agreement with D20 neutron powder data, is consistent with the CRYPAD experiment, is of the $2\mathbf{k}-\mathbf{k}'$ type, and produces eight frequencies in the μSR experiment.

To compare the proposed models with the previous neutron diffraction studies[2,20] we presented in Table III results of 1.7–3.8 K refinements. As the magnetic intensity is rather weak (Fig. 3) at 1.7 K, refinements yield worse agreement (agreement value R_m) with D20 neutron powder data. The worst agreement is for the Effantin model ($R_m=35\%$); however, the obtained ordered magnetic moment is $0.310(5)\mu_B$, which confirms the value of $0.28(6)\mu_B$ presented by Effantin *et al.*[2] within the standard deviations.

In view of the recent polemic on the question of induced magnetization near or inside the B_6 molecule[15–19] we want to add that such magnetization might be present in the AFM phase in zero field with the ordered Ce magnetic moments acting as a local field. However, our neutron diffraction experiment is a too crude probe to resolve the issue.

C. Model *D* versus μSR results

Now it is worthwhile to look on the impact of model D on μSR results in more detail. There exist two main contributions to the magnetic field at the muon site.[35] The first one originates from the dipolar fields of the surrounding magnetic moments; the second one, the contact hyperfine field, is due to the spin polarization of the conduction electrons via the RKKY mechanism. In CeB_6 the two contributions are of the same order. First, we calculated the internal fields or precession frequencies, respectively, at the muon site (d site)

TABLE IV. Muon frequencies F_{1-3} for model D under different assumptions on the hyperfine coupling constant and F_4 deduced from the experiment (Ref. 25) F_1 frequencies are obtained with an isotropic coupling constant ($A_c=1.67$ kG/μ_B), F_2 correspond to anisotropic coupling constants ($A_{c\parallel}=-4.2$ kG/μ_B, $A_{c\perp}=2.8$ kG/μ_B) deduced from Knight shift measurements in applied field (Ref. 36), and F_3 frequencies are calculated with empirical anisotropic coupling constants ($A_{c\parallel}=4.4$ kG/μ_B, $A_{c\perp}=1.67$ kG/μ_B).

Muon site			Multiplicity	F_1	F_2	F_3	F_4
				[MHz]			
0.5	0	1	8	57.5	23	77	76
1.5	0	1	16	14	18.4	30	40
2.5	0	1	8	40.3	16.4	54	60
0.5	0	0	8	1.2	0.3	1.8	2
1.5	0	0	16	4.2	2.3	6.3	4.8
2.5	0	0	8	9	3.3	12	20
0	0	0.5	8	8	19	8	8
2	0	0.5	8	3.9	10	3.9	6.5

using for the contact coupling constant the value $A_c=1.67$ kG/μ_B derived from the μ^+ Knight shift for $T>T_Q$ under the assumption that it is isotropic and temperature independent.[36] The results are presented in the column F_1 of Table IV. The three highest frequencies are lower than the experimental ones (column F_4 of Table IV); the highest reaches 57.5 MHz. A recent reinspection of the μSR Knight shift measurements,[36] assuming no induced magnetization near or outside the B_6 molecule, led to an anisotropic contact hyperfine field $\mathbf{B}_C$ depending on the angle φ between an induced Ce moment $\boldsymbol{\mu}$ and the radius vector connecting this moment with the nearest muon position (only two nearest Ce neighbors are considered):

$$\mathbf{B}_C=\sum_{i=1}^{2}(A_{c\parallel}\cos^2\varphi_i+A_{c\perp}\sin^2\varphi_i)\boldsymbol{\mu}_i, \tag{9}$$

with $A_{c\parallel}$ being a coupling constant in the direction parallel to Ce magnetic moment and $A_{c\perp}$ perpendicular to it. Near T_N one finds $A_{c\parallel}=-4.2$ kG/μ_B and $A_{c\perp}=2.8$ kG/μ_B (for $T\geqslant T_Q$, $A_{c\parallel}=6$ kG/μ_B and $A_{c\perp}\approx 1$ kG/μ_B). Using this coupling constants we obtain the frequencies presented in the column F_2 of Table IV. Due to the negative sign of $A_{c\parallel}$, dipolar and contact fields compensate each other, resulting in significantly smaller fields at the muon sites at $z=1$. The highest frequency of only 23 MHz is obtained. Better agreement with experimental results is obtained under the assumption that both coupling constants are positive. For $A_{c\parallel}=4.4$ kG/μ_B and $A_{c\perp}=1.67$ kG/μ_B the resulting frequencies are listed in the column F_3. They fit well the frequencies obtained from the experiment.[25] The discrepancy in the coupling constants deduced from the Knight shift under applied field and assumed by us may be attributed to the temperature dependence of $A_{c\parallel}$ and $A_{c\perp}$, which is not determined below T_N. Another reason might be that the coupling constants are sensitive to multipolar order, i.e., dipolar, quadrupolar and octupolar, which is different for zero and applied magnetic

fields. It is known that contact hyperfine fields at muon sites arise from the spin polarization of conduction electrons induced by magnetic moments on Ce atoms via the RKKY interactions. The anisotropy of the coupling constants reflects the anisotropy of the RKKY coupling and, correspondingly, the anisotropy of the charge distribution of $4f$ electrons which is different for the cases of zero and applied magnetic fields. The anisotropy of the coupling constants is in accord with theoretical investigations[37,38] which indicates that the RKKY interactions and spin polarization of the conduction electrons are anisotropic in CeB_6. It is worth noting that similar anisotropy has been observed in other quadrupolar ordered systems, such as UPd_3 (Ref. 39) and HoB_2C_2 (Ref. 40). In HoB_2C_2, for example, the contact coupling constant changes from an isotropic negative to an anisotropic and positive below 50 K.

Finally, we estimated the possible influence of induced boron magnetization density on the μSR results. Under assumption that the induced magnetization density is only 5% of the adjacent Ce magnetic moments, the spontaneous precession frequencies would split into narrow bands and would shift compared to the values with magnetization on Ce atoms. We can conclude that presence of induced boron magnetization density would weakly affect internal fields at muon sites.

Within presently available experimental information assuming highly anisotropic contact hyperfine coupling constants we obtain appreciable understanding of the zero-field μSR results for model *D*. The number of spontaneous frequencies, the spread of their values in the 76–2.5 MHz range, and the multiplicity of the muon sites can be explained.

D. Evolution of the AF magnetic order at low temperatures (36 mK$<T<$2.3 K)

The variation of integrated intensity of (1/4 1/4 0) and (1/4 1/4 1/2) AF reflections of $Ce^{11}B_6$ single crystal in temperature range from 36 mK to 2.3 K has been measured at the single-crystal neutron diffractometer TriCS with $\lambda = 1.18$ Å. The intensities steeply increase in the 2.3–1.2 K temperature interval Fig. 6(a) and change very little below 1.2 K.[41] The intensity of the (1/4 1/4 0) reflection increases faster compared to (1/4 1/4 1/2) as can be seen from the ratio of intensities plotted in Fig. 6(b). This means that the magnetic moments associated with $\mathbf{k}_1$ develop faster than those associated with $\mathbf{k}_1'$. Such behavior might have a common origin with the peculiar behavior of two spontaneous μ^+ Larmor precession frequencies shown in Fig. 1 of Ref. 25. Within the developed model *D* the two frequencies correspond to muons located at the (0 0 1/2) and (2 0 1/2) sites between the layers at $z=0$ and $z=1$. Based on this assumption the difference between magnetic moments values at the layers at $z=0$ and $z=1$, reflecting the competition between the dipolar, quadrupolar, and octupolar ordering, develops below 1 K and not at T_N. Another reason of the peculiar behavior of two μSR frequencies might be change of the anisotropic coupling constants with temperature discussed in Sec. III C.

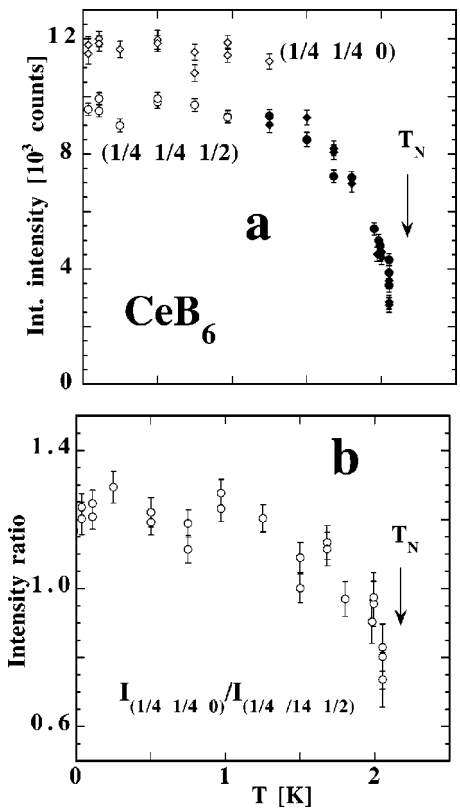

FIG. 6. (a) Temperature dependence of the observed integrated AFM intensity of (1/4 1/4 0) (diamonds) and (1/4 1/4 1/2) (circles) reflections of $Ce^{11}B_6$ single crystal in mK regime. Solid and open symbols correspond to two different experiments. (b) Temperature dependence of the ratio of the (1/4 1/4 0) and (1/4 1/4 1/2) intensities.

E. Model *D* versus theoretical studies

The arrangement of the magnetic moments within one layer in model *D* is compatible with the O_{xy}-type AFQ ordering: the relative orientation of dipolar and quadrupolar moments is the same within the layer. However, it is not the case for the three-dimensional arrangement. The dipolar moments at $z=0$ should be rotated 90° to have the same relative orientation to quadrupoles as in the layer at $z=1$. It seems that for nearest-neighboring atoms of different layers the AFM coupling is stronger than the dipolar-quadrupolar coupling. In addition the magnetic moment values are different for the two layers. We suggest that this complicated structure is caused by competition between the dipolar, quadrupolar, and octupolar ordering. The theoretical study[23] showed that to account for the orthogonal arrangement of nearest-neighbor magnetic moments in the AFM state of CeB_6 the interactions of the next-nearest-neighbor dipole and octupole moments are required.

According to these calculations the electric quadrupolar and magnetic octupolar moments are aligned along the same direction, while dipolar and octupolar magnetic moments are orthogonal to each other; pure dipole-dipole interactions would prefer a collinear alignment. The competition of these comparable in strength interactions might lead to suppression to the ordered dipolar moment at the $z=0$ layer and to the

amplitude modulation of the magnetic moment within the layers. Interestingly from the calculations it follows that an incommensurate octupole ordering should be realized for a certain set of parameters. Kusunose and Kuramoto[23] proposed that such ordering is realized in the single-domain AFM phase III′ (Ref. 20) in small magnetic fields. Our result suggests that the incommensurate octupole ordering may occur already in the AFM phase in zero field leading to the amplitude modulation of the magnetic moment within the layers.

IV. SUMMARY

We have investigated powder and single-crystal $Ce^{11}B_6$ by means of neutron diffraction at low temperatures and zero field. We failed to detect any deviation from cubic $Pm\overline{3}m$ symmetry at the AFQ and AFM states within the precision of the high-resolution neutron powder diffraction and neutron single-crystal spherical polarimetry. The Effantin model[2] gave rather poor fit to our high-intensity neutron powder diffraction data collected at 60 mK. Therefore, we revised the zero-field AFM structure based on findings of four experimental techniques—high-intensity neutron powder diffraction, neutron single-crystal spherical polarimetry, single-crystal diffraction at applied field,[20] and zero-field μSR.[25] The best model of magnetic structure (model D) comprised two layers at $z=0$ and $z=1$ with different moment values, each of the layers has additional modulation of moment values. We propose that this complex structure emerges from a competition between dipolar, quadrupolar, and octupolar interactions. Development of the dipolar and octupolar order with orthogonal easy axes within already established quadrupolar order leads to suppression of the ordered dipolar magnetic moment at one of the layers. We suggest that the incommensurate octupole ordering may occur in the AFM phase.

We want to emphasize that the available experimental results are not sufficient to distinguish with certainty between the several models introduced in Sec. III A. A very precise single-crystal neutron diffraction experiment and further μSR studies at low fields would be desirable to confirm that model D is in fact the correct choice. Moreover, the true crystal structure in the zero-field AFQ state should be established and the type of multi-**k** structure of the zero-field AFM state should be unambigously determined by future synchrotron x-ray studies on single crystals.

ACKNOWLEDGMENTS

Support by the Swiss National Foundation is gratefully acknowledged. The work was performed at SINQ, Paul Scherrer Institute, Villigen, Switzerland, and at ILL, Grenoble, France. We thank for the expert technical assistance by Dr. M. Zolliker, PSI and S. Pujol, ILL. Dr. V. Pomjakushin, PSI is acknowledged for the computer code for calculation of dipolar fields.

*Corresponding author. FAX: +41 56 310 2939. Electronic address: Oksana.Zaharko@psi.ch

[1] S. Horn, F. Steglich, M. Loewenhaupt, H. Scheuer, W. Felsch, and K. Winzer, Z. Phys. B: Condens. Matter **42**, 125 (1981).
[2] J.M. Effantin, J. Rossat-Mignod, P. Burlet, H. Bartholin, S. Kunii, and T. Kasuya, J. Magn. Magn. Mater. **47-48**, 145 (1985).
[3] F. Yakhou, V. Plakhty, H. Suzuki, S. Gavrilov, P. Burlet, L. Paolasini, C. Vettier, and S. Kunii, Phys. Lett. A **285**, 191 (2001).
[4] H. Nakao, KI. Magishi, Y. Wakabayashi, Y. Murakami, K. Koyama, K. Hirote, Y. Endoh, and S. Kunii, J. Phys. Soc. Jpn. **70**, 1857 (2001).
[5] A. Takase, K. Kojima, T. Komatsubara, and T. Kasuya, Solid State Commun. **36**, 461 (1980).
[6] M. Sera, H. Ichikawa, T. Yokoo, J. Nishi, K. Kakurai, and S. Kunii, Phys. Rev. Lett. **86**, 1578 (2001).
[7] R. Shiiina, H. Shiba, and P. Thalmeier, J. Phys. Soc. Jpn. **66**, 1741 (1997).
[8] R. Shiina, O. Sakai, H. Shiba, and P. Thalmeier, J. Phys. Soc. Jpn. **67**, 941 (1998).
[9] O. Sakai, R. Shiiina, H. Shiba, and P. Thalmeier, J. Phys. Soc. Jpn. **67**, 3005 (1997).
[10] O. Sakai, R. Shiiina, H. Shiba, and P. Thalmeier, J. Phys. Soc. Jpn. **68**, 1364 (1999).
[11] M. Sera and S. Kobayashi, J. Phys. Soc. Jpn. **68**, 1664 (1999).
[12] T. Kasuya, J. Magn. Magn. Mater. **174**, L28 (1997).
[13] S. Lovesey, J. Phys.: Condens. Matter **14**, 4415 (2002).
[14] H. Yamauchi, H. Onodera, K. Ohoyama, T. Onimaru, M. Kasaka, M. Ohashi, and Y. Yamaguchi, J. Phys. Soc. Jpn. **68**, 2057 (1999).
[15] M. Saitoh *et al.* J. Phys. Soc. Jpn. **71**, 2369 (2002).
[16] K. Hanzawa, J. Phys. Soc. Jpn. **69**, 510 (2000).
[17] K. Hanzawa, J. Phys. Soc. Jpn. **70**, 1900 (2001).
[18] A. Schenck, F.N. Gygax, and S. Kunii, Phys. Rev. Lett. **89**, 037201 (2002).
[19] F. Givord, J.-X. Boucherle, P. Burlet, B. Gillon, and S. Kunii, J. Phys.: Condens. Matter **15**, 3095 (2003).
[20] J.M. Effantin, P. Burlet, J. Rossat-Mignod, S. Kunii, and T. Kasuya, in *Proceedings of International Conference on Valence Instabilities, Zürich, 1982*, edited by P. Wachter and H. Boppart (North-Holland, Amsterdam, 1982), p. 559.
[21] Yu.A. Izyumov and V.E. Naish, J. Magn. Magn. Mater. **12**, 239 (1979).
[22] W. Sikora, in *Symmetry and Structural Properties of Condensed Matter, Zajaczkowo, 1999*, edited by T. Lulek *et al.* (World Scientific, Singapore, 1999), p. 484.
[23] H. Kusunose and Y. Kuramoto, J. Phys. Soc. Jpn. **70**, 1751 (2001).
[24] R. Feyerherm, A. Amato, F.N. Gygax, A. Schenck, Y. Onuki, and N. Sato, Physica B **194–196**, 357 (1994).
[25] R. Feyerherm, A. Amato, F.N. Gygax, A. Schenck, Y. Onuki, and N. Sato, J. Magn. Magn. Mater. **140-144**, 1175 (1995).
[26] J. Rossat-Mignot, P. Burlet, T. Kasuya, S. Kunii, and T. Kamatsubara, Solid State Commun. **39**, 471 (1981).
[27] J. Rodriguez-Carvajal, Physica B **192**, 55 (1993).
[28] F. Tasset, P.J. Brown, E. Lelièvre-Berna, T. Roberts, S. Pujol, J. Allibon, and E. Bourgeat-Lami, Physica B **267-268**, 69 (1999).
[29] P. Fischer, G. Frey, M. Koch, M. Könnecke, V. Pomjakushin, J. Schefer, R. Thut, N. Schlumpf, R. Bürge, U. Greuter, S. Bondt,

and E. Berruyer, Physica B **276-278**, 146 (2000).
[30] R. Schefzyk, M. Peschke, F. Steglich, and K. Winzer, J. Magn. Magn. Mater. **63-64**, 67 (1987).
[31] Henceforth the crystallographic unit cell is used.
[32] As no ferromagnetic component was reported from macroscopic magnetization measurements and no lattice distortion was detected from our HRPT experiment we attribute additional intensities at the nuclear positions to reduction of the extinction due to the AFQ and AFM ordering. The absence of ferromagnetism is confirmed by the CRYOPAD experiment as well.
[33] P.J. Brown, Physica B **192**, 14 (1993).
[34] Yu. A. Izyumov, *Neutron Diffraction of Magnetic Materials* (Consultants Bureau, New York, 1991).
[35] A. Schenck, in *Muon Science*, edited by S.L. Lee, R. Cywinski, and S.H. Kilcoyne (Insitute of Physics, Bristol, 1999).
[36] A. Schenck (unpublished).
[37] P. Schlottmann, Phys. Rev. B **62**, 10 067 (2000).
[38] Y. Kuramoto and K. Kubo, J. Phys. Soc. Jpn. **71**, 2633 (2002).
[39] A. Schenck, F.N. Gygax, and K.A. McEwen, J. Phys.: Condens. Matter **14**, 4595 (2002).
[40] F. de Lorenzi, N.F. Gygax, A. Schenck, A. Tobo, and H. Onodera, Physica B **326**, 581 (2003).
[41] Note that raw data presented in Fig. 6(a) are not corrected for temperature-independent factors, such as the Lorentz factor and absorption. This allows us to follow thermal evolution of the two reflections, but hampers direct comparison with the powder data.